Rheol Acta
DOI 10.1007/s00397-008-0280-5

ORIGINAL CONTRIBUTION

Relaxation patterns of long, linear, flexible, monodisperse polymers: BSW spectrum revisited

Christian Friedrich · Wolfgang Waizenegger · Horst Henning Winter

Received: 19 December 2007 / Accepted: 22 March 2008
© Springer-Verlag 2008

Abstract Theoretical predictions for the dynamic moduli of long, linear, flexible, monodisperse polymers are summarized and compared with experimental observations. Surprisingly, the predicted 1/2 power scaling of the long-time modes of the relaxation spectrum is not found in the experiments. Instead, scaling with a power of about 1/4 extends all the way up to the longest relaxation times near $\tau/\tau_{\max} = 1$. This is expressed in the empirical relaxation time spectrum of Baumgaertel-Schausberger-Winter, denoted as "BSW spectrum," and justifies a closer look at the properties of the BSW spectrum. Working with the BSW spectrum, however, is made difficult by the fact that hypergeometric functions occur naturally in BSW-based rheological material functions. BSW provides no explicit solutions for the dynamic moduli, $G'(\omega)$, $G''(\omega)$, or the relaxation modulus $G(t)$. To overcome this problem, close approximations of simple analytical form are shown for these moduli. With these approximations, analysis of linear viscoelastic data allows the direct determination of BSW parameters.

C. Friedrich (✉) · W. Waizenegger
Institut für Makromolekulare Chemie und
Freiburger Materialforschungszentrum (FMF),
Albert-Ludwigs-Universität Freiburg i. Br.,
Stefan-Meier Str. 21, 70104, Freiburg, Germany
e-mail: christian.friedrich@fmf.uni-freiburg.de

H. H. Winter
Chemical Engineering Department and
Polymer Science and Engineering Department,
University of Massachusetts/Amherst,
Amherst, MA 01003, USA
e-mail: winter@ecs.umass.edu

Keywords Polymer melts · BSW-spectrum · Reptation · Polyisoprene

Introduction

Much emphasis has been devoted to finding relations between molecular architecture of complex materials and corresponding relaxation functions. Early experimental studies and theoretical predictions focused on linear polymers. Research on other architectures and compositions followed, such as star-shaped polymers, H-polymers, combs, pom-poms, polymer blends, soft glasses, gels, and a few other complex materials. Between all of these, the long, linear, flexible, monodisperse polymers (LLFMP) take a leading role for the understanding of polymer dynamics.

The relaxation patterns of LLFMP are believed to be independent of chemical composition. The same patterns were found experimentally with highly entangled polystyrene (PS; Onogi et al. 1970; Schausberger et al. 1985), polybutadiene (PB; Baumgärtel et al. 1992), and polyisoprene (PI) (Abdel-Goad et al. 2004). Complications arise from the fact that the usual rheological material functions, such as relaxation modulus $G(t)$ and dynamic moduli $G'(\omega)$, $G''(\omega)$, do not express themselves in an obvious mathematical format that would lend itself to be extracted intuitively from the experimental data. Relaxation time spectra provide an easier and more compact representation of LLFMP viscoelasticity and will be used throughout this study.

This study focuses on the entanglement and terminal relaxation behavior of LLFMP. The main material-specific parameters are the plateau modulus, G_N^0, and the longest relaxation time, $\tau_{\max}$. G_N^0 typically defines

the entanglement molecular weight $M_e = \rho RT/G_N^0$ of a polymer (Ferry 1980). Molecular mass effects depend on the number of entanglements, $Z = M/M_e$, where M is the molar mass of the monodisperse polymer.

The experimentally observed relaxation behavior of LLFMP has been successfully expressed by the so-called BSW spectrum (Baumgärtel et al. 1990). The BSW spectrum stands out because of its simplicity and its closeness to experimental observation. In spite of being purely empirical without any known theoretical backing, BSW can ideally serve as reference for exploring the properties of LLFMP spectra that were theoretically predicted from molecular dynamics. Such analysis and exploration will be pursued below. A BSW-based analysis, however, leads quickly to hypergeometric functions as shown by Carri and Winter (1997).

To overcome this obstacle of intractability, we suggest to rearrange hypergeometric functions [that occur naturally in $G(t)$, $G'(\omega)$, and $G''(\omega)$] into a product of two functions each. The first function in these factorials is written in a format that captures the asymptotes at short and long times. The second function defines the shape of the transition from short to long. Such mathematical form makes it easier to treat rheological material functions analytically and to gain an intuitive understanding of the underlying physics.

Analytical expressions for the relaxation time spectrum

The linear viscoelastic behavior of complex materials is known to be governed by Boltzmann's equation, which can be written as

$$\sigma(t) = \int_{-\infty}^{t} dt'\, G\left(t - t'\right)\, 2D\left(t'\right). \tag{1}$$

$\sigma(t)$ is the extra stress at time t and $2D(t')$ the rate of deformation at all times t' in the past, $-\infty < t' < t$. The density is assumed to be constant so that the relaxation modulus $G(t)$ is the only material function needed to characterize the equilibrated material structure. Instead of $G(t)$, equivalent material functions may be chosen to express relaxation. One such function is the relaxation time spectrum $H(\tau)$, which is related to the relaxation modulus $G(t)$ by an implicit function

$$G(t) = \int_0^{\infty} \frac{d\tau}{\tau}\, H(\tau)\, e^{-t/\tau}. \tag{2}$$

Similar implicit relations exist for relating $H(\tau)$ to other linear viscoelastic material functions such as the dynamic moduli

$$G'(\omega) = \int_0^{\infty} \frac{d\tau}{\tau}\, H(\tau)\, \frac{\omega^2\tau^2}{1+\omega^2\tau^2};$$

$$G''(\omega) = \int_0^{\infty} \frac{d\tau}{\tau}\, H(\tau)\, \frac{\omega\tau}{1+\omega^2\tau^2}. \tag{3}$$

These material functions are most sensitive to small variations of molecular architecture and composition.

Of the many possible molecular architectures and compositions, most deeply understood is the relaxation of LLFMP, i.e., of polymers with long, linear, flexible molecules of uniform molar mass M. Linear viscoelastic data and theoretical predictions agree quite well for this special class of highly entangled polymers. In the following, we will further explore their linear viscoelastic properties, especially their relaxation patterns in the entanglement and flow regime. However, we neglect short-time contributions to the spectrum, e.g., the onset to glass transition at short times or high frequencies. These contributions are governed by different physical laws and require a separate study. Fast modes might be modeled either empirically by a second power law as done in the original BSW-model or structurally by adding Rouse modes. This would exceed the scope of this study.

Baumgärtel et al. (1990) evaluated experimental $G'(\omega)$,$G''(\omega)$) data of LLFMP and determined the general form of the relaxation functions by inverting these data from the frequency domain to the time domain. They found that, within experimental error, a simple power-law spectrum is able to express all details of published $G'(\omega)$,$G''(\omega)$) data of Schausberger et al. (1985) and their own (Baumgärtel et al. 1992). Based on this observation, they proposed a relaxation time spectrum (denoted as "BSW-spectrum")

$$H(\tau) = \begin{cases} n_e\, G_N^0 \left(\dfrac{\tau}{\tau_{\max}^{\mathrm{BSW}}}\right)^{n_e} & \text{for} \quad \tau \le \tau_{\max}^{\mathrm{BSW}} \\ 0 & \text{for} \quad \tau_{\max}^{\mathrm{BSW}} < \tau \end{cases}, \tag{4}$$

which contains no free parameters. G_N^0 is the plateau modulus and $(-n_e)$ is the slope of $\log G''(\log\omega)$ in the entanglement region. Experiments show that exponent n_e adopts values in the range of n_e = 0.20 to 0.25. The longest relaxation time increases with molar mass as

$$\tau_{\max}^{\mathrm{BSW}} = \tau_0 Z^{3.4} \text{ with } Z = M/M_e, \tag{5}$$

where 3.4 is the typical experimentally found exponent value. τ_0 is a time constant for the crossover from the entanglement region to the glass transition as defined by Carri and Winter (1997).

Rheological experiments have been compared extensively with BSW predictions. Baumgärtel et al. (1990, 1992) and Jackson et al. (1994) identified the cut-off relaxation time of the spectrum with the reptation time of the polymers under consideration (PS, PB, PI). More recently, Abdel-Goad et al. (2004) confirmed this finding for other model polymers and, furthermore, showed for the highest molecular weights that the phenomenologically determined (by fitting) cut-off times change their Z-dependence to the expected reptation limit. They confirmed that the BSW spectrum captures all essential features in the behavior of LLFMP irrespective of their molecular weight (for the samples used). This brings us to the conclusion that BSW must be an acceptable approximation of the theoretically justified relaxation time spectra. The validity of this assumption will be explored in the following.

The experimentally observed BSW-spectrum is close to an earlier theoretical prediction of Doi (1981) who proposed a relaxation time spectrum for LLFMP, $H^D(\tau)$:

$$H^D(\tau) = \begin{cases} H^D_{\text{fluct}}(\tau) & for \quad \tau < \dfrac{\tau_d^\infty}{Z} \\ H^D_{\text{rept}}(\tau) & for \quad \dfrac{\tau_d^\infty}{Z} \le \tau \le \tau_d^D \\ 0 & for \quad \tau > \tau_d^D \end{cases}, \tag{6}$$

with $\tau_d^D \left(\equiv \tau^D_{\max}\right) = \tau_d^\infty \left(1 - Z^{-1/2}\right)^2$, $\tau_d^\infty = 3\tau_e Z^3$, and $Z = M/M_e$. τ_e is called the Rouse time of a chain segment between entanglements. The first term in Eq. 6,

$$H^D_{\text{fluct}}(\tau) = \frac{1}{2} G_N^0 \left(\frac{\tau}{Z\tau_d^\infty}\right)^{1/4}, \tag{7}$$

expresses relaxation due to "contour-length fluctuations." Contour-length fluctuation is viewed as a fast process in which linear chains contract and expand again, thereby randomizing the orientation of chain ends and relaxing the corresponding stress components. These motions are effective in relaxing the chain ends. The fast relaxing fluctuations contribute to the frequencies in the entanglement region and entail the characteristic G''-slope of 0.25 (in the typical log–log representation).

This is different for the innermost parts of the molecular chains, which maintain their orientation for a comparably long time and, thus, continue to contribute longer to the stress. The chains' center section relaxes, as expressed by the second term in Eq. 6,

$$H^D_{\text{rept}}(\tau) = \frac{1}{2} G_N^0 \left(\frac{\tau}{\tau_d^\infty}\right)^{1/2}, \tag{8}$$

in a longitudinal diffusion motion (reptation) in the temporary network of the other chains. Reptation is effective in relaxing all induced orientations and, therefore, represents the terminal relaxation process. Complete relaxation requires reptation by a distance as large as the chain's own size. The exponent value of 1/2 belongs to the dynamics of linear diffusion.

The relaxation spectrum representation of this reptation dynamics was first given by Doi (1974). The reptation part of the spectrum is expected to define the terminal properties of the sample including the characteristic slopes of dynamic moduli at frequencies smaller than the inverse of the terminal relaxation time, $\left(\tau^D_{\max}\right)^{-1}$.

Another very similar spectrum is that of Milner and McLeish (1998), who predicted the relaxation time spectrum, $H^{\text{MM}}(\tau)$, of LLFMP by taking their theory for monodisperse star-shaped polymers in the limit of two-armed stars:

$$H^{\text{MM}}(\tau) = \begin{cases} H^{\text{MM}}_{\text{fluct}}(\tau) + H^{\text{MM}}_{\text{rept}}(\tau) & \text{for} \quad \tau \le \tau_d^{\text{MM}} \\ 0 & \text{for} \quad \tau_d^{\text{MM}} < \tau \end{cases} \tag{9}$$

with spectra for contour-length fluctuations and reptation

$$H^{\text{MM}}_{\text{fluct}}(\tau) = \frac{1}{2} s_d \, G_N^0 \left[1 - s_d \left(\frac{\tau}{\tau_d^{\text{MM}}}\right)^{1/4}\right] \left(\frac{\tau}{\tau_d^{\text{MM}}}\right)^{1/4}$$

$$\approx \frac{1}{2} s_d \, G_N^0 \left(\frac{\tau}{\tau_d^{\text{MM}}}\right)^{1/4}$$

$$H^{\text{MM}}_{\text{rept}}(\tau) = \frac{1}{2} G_N^0 \, (1 - s_d)^2 \left(\frac{\tau}{\tau_d^{\text{MM}}}\right)^{1/2}. \tag{10}$$

The length s_d is defined as the fractional distance from the free end of the chain beyond which reptation becomes the faster process, in comparison to contour length fluctuations.

The Z-dependence can be found by solving the equation, $(1 - s_d)^2 = a_d Z s_d^4$ with parameter $a_d = 225\,\pi^3/256 = 27.25$:

$$s_d(Z) = \frac{\sqrt{1 + 4\sqrt{a_d Z}} - 1}{2\sqrt{a_d Z}} \cong \frac{1}{(a_d Z)^{1/4}} - \frac{1}{2\,(a_d Z)^{1/2}}. \tag{11}$$

Milner and McLeish defined the terminal relaxation time similarly to Doi:

$$\tau_d^{\text{MM}} \left(\equiv \tau^{\text{MM}}_{\max}\right) = \tau_d^\infty \left(1 - s_d(Z)\right)^2. \tag{12}$$

However, their functional dependence yields better agreement between experimentally observed terminal

relaxation times and theory than Doi's (1981) presentation.

Having such explicit functional representation on hand, we are able to compare the spectra quantitatively; see Fig. 1. Direct comparison is possible since all spectra are normalized to satisfy the well-known property

$$\int_0^\infty \frac{d\tau}{\tau}\,\frac{H(\tau)}{G_N^0} = 1. \tag{13}$$

The maximal relaxation times of the three different spectra in Fig. 1 are assumed to be identical, $\tau_{\max} \equiv \tau_{\max}^{\mathrm{BSW}} = \tau_{\max}^{\mathrm{Doi}} = \tau_{\max}^{\mathrm{MM}}$.

The differences between the spectra in Fig. 1 are rather subtle. Common to all three spectra is their limiting behavior at short relaxation times according to $t^{1/4}$. This yields the commonly observed behavior $G'' \propto \omega^{-1/4}$ in the plateau region. The difference between the spectra concerns the longest relaxation modes and, especially, the transition from the fluctuation determined part of the spectrum, $H_{\mathrm{fluct}}(\tau)$, to the terminal part, $H_{\mathrm{rept}}(\tau)$. For the Doi (1981) spectrum and the MM spectrum, the Rouse and terminal relaxation times are well separated ($Z > 10$) in Fig. 1. They include the predicted slopes of 0.5 in the reptation limit near $\tau/\tau_{\max} = 1$.

Figure 2 compares measured dynamic moduli of PI with predictions of the three models that were summarized above. Especially near the maximum of G'', the shape of the curves deviates significantly from the

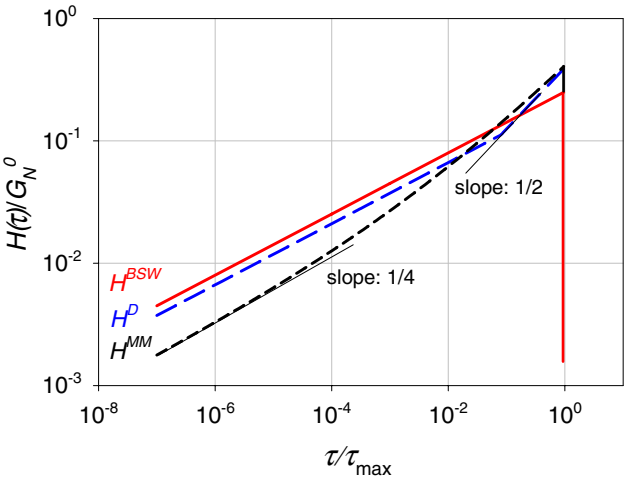

Fig. 1 Relaxation time spectrum, $H(\tau)$, for LLFMP as found experimentally (BSW spectrum) and as predicted by Doi (1981, 1983) and by Milner and McLeish (1998). The relaxation time spectrum is normalized with the plateau modulus, $H(\tau)/G_N^0$, and the longest relaxation time, $\tau/\tau_{\max}$. Parameter values are $n_e = 0.25$ and $Z = 20$

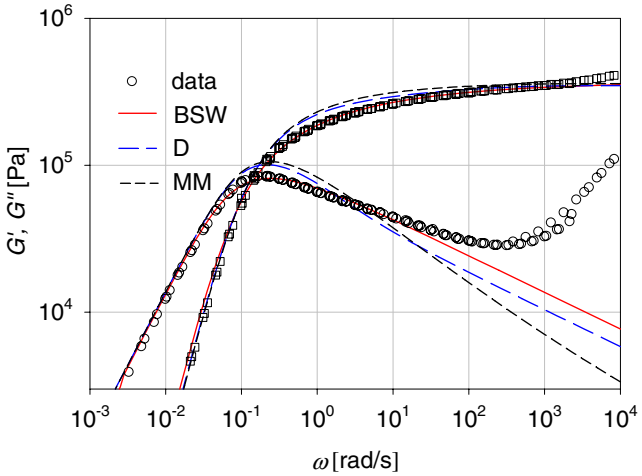

Fig. 2 Experimental data of Abdel-Goad et al. (2004) for PI300K ($Z = 49$) with calculations on the basis of three different relaxation time spectra and BSW parameters of Abdel-Goad et al. (2004): $\tau_{\max}^{\mathrm{BSW}} = 18s$, $G_N^0 = 372,000\mathrm{Pa}$. For the two other models, we used $\tau_{\max}^{\mathrm{Doi}} = \tau_{\max}^{\mathrm{MM}} = 13s$ to obtain merging curves in the terminal regime. τ_e was set to 2×10^{-5} s

experimental observation. The experimental data do not show the transition to the reptation limit in the approach of $\tau/\tau_{\max} = 1$, and this in spite of the relatively high molecular weight ($Z = 49$). Other published experiments also lack a transition to the reptation limit of 0.5.

From the three spectra above, the best representation of G'' and G' near $G''_{\max}$ is found with the empirical BSW model. Figure 2 shows that, in spite of its simple mathematical form (constant slope of about 0.25, no transition to a slope of 0.5 near $\tau/\tau_{\max} = 1$), the BSW spectrum captures the essential features of the dynamic moduli. This important property of BSW justifies a more detailed study of its dynamic material functions and a search for a simpler representation of BSW-based material functions.

Hypergeometric functions for G′, G″, and approximate solution

The BSW-spectrum solutions for Eq. 3 result in (Carri and Winter 1997):

$$G'(\omega) = n_e G_N^0 (\omega\tau_{\max})^2 \times \frac{1}{2+n_e} F\left(1, 1+\frac{n_e}{2}; 2+\frac{n_e}{2}; -(\omega\tau_{\max})^2\right), \tag{14}$$

$$G''(\omega) = n_e G_N^0 \omega\tau_{max} \frac{1}{1+n_e} \times F\left(1,\ \frac{1+n_e}{2};\ \frac{3+n_e}{2};\ -(\omega\tau_{max})^2\right). \quad (15)$$

Hypergeometric functions, $F(.,.;.;.)$, of different arguments occur naturally in the solution. Fortunately, such hypergeometric functions can be transformed into related hypergeometric functions of different form (Abramowitz and Stegun 1984). We take advantage of this property and express the corresponding hypergeometric functions in a more convenient form. It is possible to transform the hypergeometric functions of Eqs. 14 and 15 into a product of two functions

$$F\left(1, b'; c'; -x^2\right) = \frac{1}{1+x^2}\ F\left(1, c'-b'; c'; \frac{x^2}{1+x^2}\right) \quad (16)$$

$$F\left(1, b''; c''; -x^2\right) = \frac{1}{\left(1+x^2\right)^{b''}} F\left(b'', c''-1; c''; \frac{x^2}{1+x^2}\right), \quad (17)$$

with $x = \omega\tau_{max}$, in which the first function captures the slope at high and low frequencies (see Appendix 1). Multiplied with these are the new hypergeometric functions, $F\left(1, .\,; .\,; x^2/\left(1+x^2\right)\right)$, which we called "shape functions" since they define the shape of G' and G'' in the transition region from low to high frequencies. Parameters belonging to G' or G'' are marked by a single or double apostrophe, respectively.

While the shape functions are also of hypergeometric nature, they adopt a format that is much simpler than before: they approach a constant limiting value at both frequency limits (see below) and they govern a finite domain $0 < x^2/\left(1+x^2\right) < 1$. In comparison, the original hypergeometric functions in Eqs. 14 and 15 govern the domain [0,∞]. This added simplicity makes it possible to expand the newly defined hypergeometric functions in a convenient polynomial expression.

The transformations result in compact approximations for G' und G'':

$$G'_{appr}(x) = G_N^0 \cdot \frac{x^2}{1+x^2} \cdot g_1(n_e, x), \quad (18)$$

$$G''_{appr}(x) = G_N^0 \cdot \frac{x}{\left(1+x^2\right)^{(1+n_e)/2}} \cdot g_2(n_e, x), \quad (19)$$

with the approximated shape functions

$$g_1(n_e, x) = \frac{n_e}{2+n_e} F\left(1, 1; \frac{4+n_e}{2}; \frac{x^2}{1+x^2}\right) \cong a_1 - \frac{b_1}{\left(1+\left(x/x_1\right)^{8n_e}\right)^{\frac{1}{8}}}, \quad (20)$$

$$g_2(n_e, x) = \frac{n_e}{1+n_e} F\left(\frac{1+n_e}{2}, \frac{1+n_e}{2}; \frac{3+n_e}{2}; \frac{x^2}{1+x^2}\right) \cong a_2 - \frac{b_2}{\left(1+\left(x/x_2\right)^{8n_e}\right)^{\frac{1}{2}}}. \quad (21)$$

The parameter values in the approximation functions depend on the value of n_e in the following way:

$$a_1 = 1, b_1 = \frac{2}{2+n_e}, x_1 = 46.3n_e^2 - 35.98n_e + 7.7 \text{ and}$$

$$a_2 = \frac{n_e\pi/2}{\cos\left(n_e\pi/2\right)},\ b_2 = a_2 - \frac{n_e}{1+n_e},\ x_2 = 4.5\,n_e^2 + 2.79\,n_e + 0.95.$$

These parameters were obtained by minimizing the deviation from the full BSW solution of Carri.

In Fig. 3, we visualize the shape functions g_1 and g_2 for the same parameters as in Fig. 2. The sigmoidal character of both functions can clearly be recognized. Interestingly, the transition is much sharper for G'' than for G'.

The relative error between BSW and the approximative functions, Eqs. 18 and 19,

$$\varepsilon_{1(2)} = \frac{G'^{(\prime)}_{BSW} - G'^{(\prime)}_{app}}{G'^{(\prime)}_{BSW}} \quad (22)$$

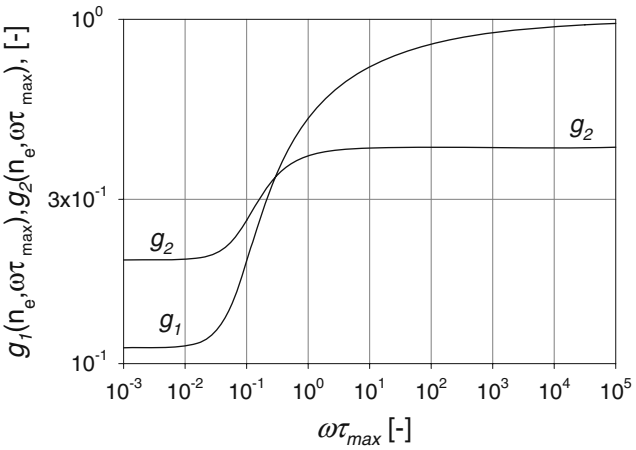

Fig. 3 Shape functions calculated for $n_e = 0.25$ and $\tau_{max} = 18$ s

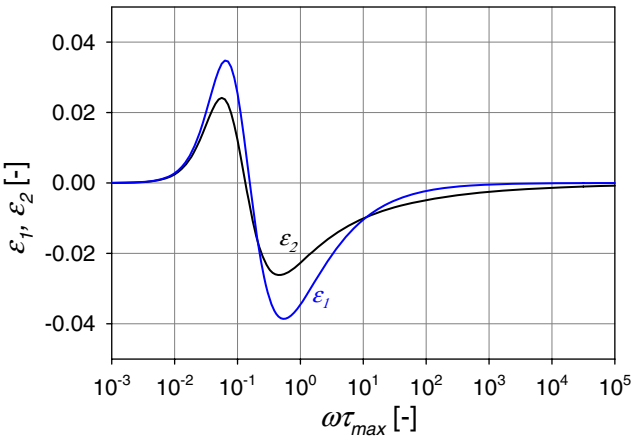

Fig. 4 Deviations between the full and approximated BSW models at the example of data given in Fig. 2

is too small to be seen in the plot for the moduli. Figure 4 shows the error in a separate plot.

Discussion

The most striking result is the almost perfect agreement between linear viscoelastic data as presented by dynamic moduli and model calculations based on the BSW spectrum. Although very simple, the BSW spectrum captures all essential features of the linear viscoelastic properties of LLFMP. Obviously, the details for the transition from early chain end fluctuations to reptation of the whole chain embedded in the Doi or Milner/McLeish spectra do not show up in rheological measurements to the extent foreseen by these authors. This raises the question why the classical linear diffusion, as expressed in reptation, does not show in the linear viscoelastic data.

This result might be interpreted differently: The BSW spectrum is a very simple approximation of the two other spectra. Therefore, BSW includes all important processes. At the simplest possible way, the BSW spectrum reflects the basic physics, which consist of a transition from chain end fluctuations, characterized by the well known $\tau^{-1/4}$ dependence, in the early stage of relaxation to a reptation process, whose spectrum is characterized by $\tau^{-1/4}\ \ h(\tau_{\max}-\tau)$, having an exponent of 1/4 instead of 1/2. Here, $h()$ is the Heaviside unit step-function. Assuming that reptation itself can be a sub-diffusive process, such an explanation is conceivable.

Another interesting observation is the surprisingly broad transition from the entanglement region to the flow region. This is especially visible with the shape function of the storage modulus g_1 (see example in Fig. 3), which changes by almost a decade in magnitude and over about seven decades in frequency (from $\omega = 10^{-2}$ to 10^5 rad/s). The broad transition of G' is especially visible since function

$$\frac{(\omega\tau_{\max})^2}{1+(\omega\tau_{\max})^2}$$

for the low ω and high ω asymptotes (see Eq. 18) transits very sharply near $\omega\tau_{\max} = 1$, so that all the broadening of the transition is expressed through the shape function g_1.

The broad transition also exists for G'', but it is less visible in the shape function g_2 (see Fig. 3) since the function for the asymptotes

$$\frac{\omega\tau_{\max}}{\left[1+(\omega\tau_{\max})^2\right]^{(1+n_e)/2}}$$

is already broad in its transition near $\omega\tau_{\max} = 1$.

Several distinct properties of $G'(\omega)$ and $G''(\omega)$, as shown in Fig. 5, can be expressed with BSW parameters. A pronounced feature is the maximum in G'' (called $G''_{\max}$), which is related to the plateau modulus by (see Appendix 3)

$$G''_{\max} = G^0_N \frac{n_e\,(1+n_e)^{0.5}\,(1+2n_e)^{0.5}}{1+2n_e+n_e^2+n_e^3}. \tag{23}$$

This means that the plateau modulus is 4.61 times higher than the maximal G'' value for the theoretically

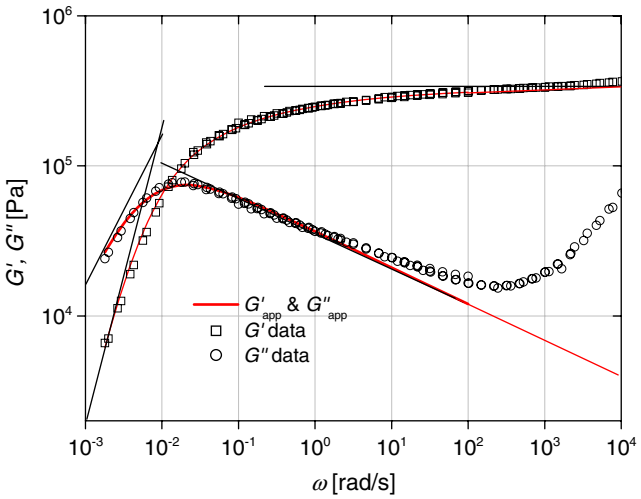

Fig. 5 Experimental data of Abdel-Goad et al. (2004) for PI730K ($Z = 122$) with calculations on the basis of approximate BSW model, Eqs. 24–26, and 27. The BSW parameters determined by simultaneous fit of both material functions are as follows: $\tau^{BSW}_{max} = 240\,s$, $G^0_N = 0.34$ MPa and $n_e = 0.24$. *The thin full lines* indicate the asymptotes according to Eqs. 25 and 27 (see Appendix 1)

predicted and often found value $n_e = 0.25$ it. Such a ratio between plateau and maximal loss modulus was found experimentally by Abdel-Goad et al. (2004) for PI and by Garcia-Franco et al. (2005) for polyolefin copolymers.

The corresponding frequency at G''_{max} is

$$\omega_{max} = \omega_{G''=G''_{max}} \approx \frac{1}{n_e \tau_{max}}. \tag{24}$$

This result means that, for LLFMP, the maximum of G'' is located around $\tau_{max}\ \omega_{max} \approx 4$. The terminal relaxation time, τ_{max}, can be determined directly from Fig. 5.

Conclusions

It is rather astounding that the experimental data suggest a constant slope of about 0.25 for the relaxation time spectrum, even in the approach of $\tau/\tau_{max} = 1$. The mathematically most simple of all available relaxation time spectra, $H \sim \tau^{n_e}$, is also the most accurate representation of the linear viscoelastic behavior of LLFMP. Not only for the polymers in this study but also for other LLFMP's in the literature, the typical features of classical reptation near $\tau/\tau_{max} = 1$ or $\omega\tau_{max} = 1$ are not observed in linear viscoelastic experiments. This suggests that, from a rheological point of view, the linear diffusion of chain segments (in tube-like constraint) does not obey Fickian dynamics.

The close representation of G^* data through the BSW spectrum makes it worthwhile to search for mathematically simple approximations of the hypergeometric functions that occur naturally when working with BSW. The approximations as proposed in this study are nearly indistinguishable from the actual BSW predictions, but they are simple to use and intuitive in their description of relaxation. In one application, the maximum in G'' could be related to the plateau modulus and the longest relaxation time in analytical expressions.

Acknowledgements HHW acknowledges the support from DFG by SFB428 and support from MRSEC NSF DMR0213695. The authors thank W. Pyckhout-Hintzen for the sharing his PI data.

Appendix 1: Asymptotes to the dynamic moduli

The approximate solution has to satisfy Eqs. 20 and 21 at low and at high frequencies, ($\omega\tau_{max} << 1$) and ($\omega\tau_{max} >> 1$). The low frequency asymptotes of the dynamic moduli of BSW are

$$G'_{\omega\tau_{max}<<1}(\omega) = \frac{n_e}{2+n_e} G_N^0 (\omega\tau_{max})^2;$$

$$G''_{\omega\tau_{max}<<1}(\omega) = \frac{n_e}{1+n_e} G_N^0 \omega\tau_{max}. \tag{25}$$

The low-frequency asymptotes intersect at (see Fig. 5)

$$\omega_x = \frac{1}{\tau_{max}} \frac{2+n_e}{1+n_e}. \tag{26}$$

The corresponding high frequency asymptotes are

$$G'_{\omega\tau_{max}>>1}(\omega) = G_N^0;$$

$$G''_{\omega\tau_{max}>>1}(\omega) = \frac{n_e \pi/2}{\cos(n_e\pi/2)} G_N^0 (\omega\tau_{max})^{-n_e}. \tag{27}$$

Appendix 2: Incomplete gamma function for $G(t)$ and approximate solution

For completeness, we present the approximation of the relaxation function obtained for BSW spectrum. Again, we start out with the expression of Carri and Winter (1997). The BSW-spectrum solution for Eq. 2,

$$G(t) = n_e G_N^0 \left(\frac{t}{\tau_{max}^{BSW}}\right)^{n_e} \Gamma\left(-n_e, \frac{t}{\tau_{max}^{BSW}}\right), \tag{28}$$

includes an incomplete Gamma function that can be replaced by a suitable approximation. The result is a polynomial expression multiplied by an exponential decay:

$$G(t)_{app} = G_N^0 \left[1 + \left(\frac{t}{n_e \tau_{max}^{BSW}}\right)^{\frac{\alpha n_e^\beta}{3}} + \left(\frac{t}{n_e \tau_{max}^{BSW}}\right)^{\alpha n_e^\beta}\right]^{-\frac{1}{\alpha n_e^\beta}} e^{-\frac{t}{\tau_{max}^{BSW}}}. \tag{29}$$

An optimized fit is achieved with $\alpha = 1.23$ and $\beta = 0.18$. The approximation is chosen such that the equation is an exact solution for the short time and the long time asymptotes (while neglecting the glass transition as stated in the beginning). These two limits are

$$G_{app}(t/\tau_{max} << 1) = G(t/\tau_{max} << 1) = G_N^0, \text{ and} \tag{30}$$

$$G_{app}(t/\tau_{max} >> 1) = G(t/\tau_{max} >> 1) = n_e G_N^0 e^{-\frac{t}{\tau_{max}^{BSW}}} \left(\frac{t}{\tau_{max}^{BSW}}\right)^{-1}. \tag{31}$$

Appendix 3: Same other interesting properties of BSW related moduli

The maximum of the loss modulus is a distinct data point from dynamic mechanical experiments. $\omega_{\max}$ is the particular frequency for which $G'' = G''_{\max} = G''(\omega_{\max})$. When predicted with BSW, $G''_{\max}$ posses properties that resemble the Maxwell model:

$$\frac{G''_{\max}}{G^0_N} = \frac{x_{\max}}{1 + x^2_{\max}} \tag{32}$$

with $x_{\max} = \omega_{\max}\, \tau_{\max}$. Although this equation is of Maxwellian structure, the Maxwell result is not recovered because, for the same material parameters, $\omega_{\max}$ is different for the Maxwell and the BSW spectra. Equation 32 can be derived from the integral equation for $G''_{\max}$,

$$\frac{G''_{\max}}{G^0_N} = n_e x^{-n_e}_{\max} \int_0^{x_{\max}} dx \frac{x^{n_e}}{1 + x^2}, \tag{33}$$

together with the defining equation for the abscissa. The condition $dG''/d\omega|_{\omega=\omega\,\max} = 0$ results in

$$-n_e x^{-1-n_e}_{\max} \int_0^{x_{\max}} dx \frac{x^{n_e}}{1 + x^2} + \frac{1}{1 + x^2_{\max}} = 0. \tag{34}$$

The solution of Eq. 34 results in the value for $x_{\max}$. For this purpose, we substitute the integral by the corresponding hypergeometric function and then transform the equation to receive the following result:

$$F\left(1, 1; \frac{n_e + 3}{2}; \frac{x^2_{\max}}{1 + x^2_{\max}}\right) = \frac{n_e + 1}{n_e}. \tag{35}$$

Again, we approximate the hypergeometric function by a simpler function and arrive at

$$\left(1 + (1 + n_e)\, x^2_{\max}\right)^{0.5} \cong \frac{n_e + 1}{n_e}, \tag{36}$$

which leads to an explicit expression for $x_{\max}$:

$$x_{\max} \cong \frac{1}{n_e}\sqrt{\frac{2n_e + 1}{n_e + 1}} \approx \frac{1}{n_e}. \tag{37}$$

Together with Eq. 32, we obtain the final result:

$$\frac{G''_{\max}}{G^0_N} = \frac{n_e\,(1 + n_e)^{0.5}\,(1 + 2n_e)^{0.5}}{1 + 2n_e + n^2_e + n^3_e}, \tag{38}$$

or

$$\frac{G''_{\max}}{G^0_N} \approx \frac{n_e}{1 + n^2_e} \tag{39}$$

that relates the value of the plateau modulus to the maximal value of the G'' for a known relaxation exponent n_e.

References

Abdel-Goad M, Pyckhout-Hintzen W, Kahle S, Allgaier J, Richter D, Fetters LJ (2004) Rheological properties of 1,4-polyisoprene over a large molecular weight range. Macromolecules 37:8135–8144

Abramowitz M, Stegun IA (1984) Pocketbook of mathematical functions. Verlag Harri Deutsch, Frankfurt/Main

Baumgärtel M, Schausberger A, Winter HH (1990) The relaxation of polymers with linear flexible chains of uniform length. Rheol Acta 29:400–408

Baumgärtel M, Derosa ME, Machado J, Masse M, Winter HH (1992) The relaxation time spectrum of nearly monodisperse polybutadiene melts. Rheol Acta 31:75–82

Carri GA, Winter HH (1997) Mapping of the relaxation patterns of polymer melts with linear flexible molecules of uniform length. Rheol Acta 36:330–344

Doi M (1974) Molecular theory of the viscoelastic properties of concentrated polymer solutions. Chem Phys Lett 26:269–272

Doi M (1981) Explanation for the 3.4 power law of viscosity of polymeric liquids on the basis of the tube model. J Polym Sci Polym Lett Ed 19:265

Doi M (1983) Explanation of the 3.4-power law for viscosity of polymeric liquids on the basis of the tube model. J Polym Sci Polym Phys 21:667–684

Ferry JD (1980) Viscoelastic properties of polymers. Wiley, New York

Garcia-Franco CA, Herrington BA, Lohse DJ (2005) On the rheology of ethylene-octene copolymers. Rheol Acta 44:591

Jackson JK, De Rosa ME, Winter HH (1994) Molecular weight dependence of relaxation time spectra for the entanglement and flow behavior of monodisperse linear flexible polymers. Macromolecules 27:2426–2431

Milner ST, McLeish TCB (1998) Reptation and contour-length fluctuations in melts of linear polymers. Phys Rev Lett 81:725

Onogi S, Masuda T, Kitagawa K (1970) Rheological properties of anionic polystyrenes. I. Dynamic viscoelasticity of narrow distribution polystyrenes. Macromolecules 3:109

Schausberger A, Schindlauer G, Janeschitz-Kriegl H (1985) Rheol Acta 24:220